Journal of Coating Science and Technology
http://www.lifescienceglobal.com/journals/journal-of-coating-science-and-technology

Preparation of Low Friction MoSe$_x$/nc-Mo Coatings Containing Spherical Mo Nanoparticles

S. Grigoriev[1], R. Romanov[2], M. Volosova[1], N. Matsnev[3] and V. Fominski[2,*]

[1]*Moscow State University of Technology "STANKIN", Vadkovskii per., 3a, Moscow 127005, Russia*

[2]*National Research Nuclear University MEPhI (Moscow Engineering Physics Institute), Kashirskoe sh., 31, Moscow 115409, Russia*

[3]*University of Technology, ul. Gagarina, 42, Korelev, Moscow 141070, Russia*

Abstract: The possibility of preparation of nanocomposite coatings consisting of a solid lubricant matrix (MoSe$_x$) and nanocrystalline metal particles (nc-Mo) was demonstrated using pulsed laser deposition from synthesized target MoSe$_2$.The particles had spherical shapes and their sizes were about 5 – 50 nm. The content of the nc-Mo nanoparticles in the MoSe$_x$/nc-Mo coatings was varied by changing the laser irradiation regimes and the conditions of expansion of the laser plume from the target to substrate. It was established that the tribological properties of the nanocomposite coatings MoSe$_x$/nc-Mo are depended on the concentration of nanoparticles in the bulk of the coatings as well as on the structure of the coating matrix. The MoSe$_x$/nc-Mo coating with increased crystalline order of matrix obtained on a steel substrate reduced the friction coefficient to ~0.04 during steel ball sliding in air of laboratory humidity. Probable mechanisms of nanoparticle formation were proposed and a role of these particles in the wear of the nanocomposite MoSe$_x$/nc-Mo coatings was discussed.

1. INTRODUCTION

Transition metal dichalcogenides (TMDs) are increasingly popular due to unique structural properties. The layered crystal structures of TMDs possess the extreme degree of anisotropy that defined their potential possibility of application for low friction (solid lubricant) coatings formation. The pure TMD coatings, such as disulfides and diselenide of molybdenum and tungsten (Mo/W)(S/Se)$_2$, were thoroughly analyzed in 80's and 90's. The investigations showed that tribological behavior of pure TMD coatings was unsuitable whenever high loads were applied to the sliding contact or tests were carried out in moisture containing atmospheres.

Recently, different possibilities to improve the tribological behavior of these coatings were examined. One of the most successful ways is to deposit a composite material associating high strength materials with self-lubricants i.e. doping of TMD coatings by other chemical elements (metals, carbon, nitrogen). The achieved results and characteristics of

the composite coatings were published in a number of reviews and original articles [1-4].

The most convenient method to prepare composite coatings is co-deposition of atomic fluxes (PVD, physical vapor deposition) which are initiated by magnetron sputtering or/and laser ablation of several targets in vacuum, inert/buffer or reactive gases [5, 6]. For this method, it is obvious that structures of composite coatings are dependent on the thermochemical properties of elements used for deposition and the kinetic conditions on substrate surfaces i.e. substrates temperature. The possibilities of structural characteristics (architecture/design) modification for coatings prepared by atomic co-deposition are strongly restricted.

The development of new methods is one of the most pressing problems of PVD technology involving the deposition of new TMD-based composite coatings with original structures and improved tribological properties. In this work the experimental studies of laser-based processes have been performed for the preparation of new composite coatings MoSe$_x$/nc-Mo consisted of the solid lubricant MoSe$_2$, which is a typical representative of TMD materials, and the hard metallic nanocrystals (nc-Mo). Coatings were formed by pulsed laser

*National Research Nuclear University MEPhI (Moscow Engineering Physics Institute) Kashirskoe sh., 31, Moscow 115409, Russia; Tel: +7 903 242 2154; E-mail: VYFominskij@mephi.ru

deposition (PLD) of a complex flux containing the atomic component (Mo, Se) and nanoparticles (Mo). The Mo nanoparticles were torn from the $MoSe_2$ target during pulsed laser irradiation and deposited on the substrate. The inert buffer gas (argon, Ar) was used to change the content of nanoparticles in the coatings. The gas has scattered the atomic flux away from the substrate, but the gas did not influence the flux of nanoparticles.

It should be noted that the formation of metallic nanoparticles during pulsed laser deposition of TMD coatings has been found in a number of studies [7-9]. Nevertheless, the mechanism of nanoparticle formation has not been studied, and the methods of regulation of their concentration in a bulk of composite TMD-based coatings have not been developed.

2. EXPERIMENTAL DETAILS

The $MoSe_2$ target for PLD was manufactured by means of cold compacting technology under the pressure of 600 MPa using $MoSe_2$ powder obtained by self-propagating high-temperature synthesis. The $MoSe_2$ powder was synthesized from Mo powder, 99.93% purity and particle size of 1–4 μm, and Se powder, 99.997% purity. The surface of the pressed target $MoSe_2$ was treated mechanically (grinding, polishing) and washed with the alcohol.

An electro-optically Q-switched yttrium-aluminium-garnet laser (wavelength 1.06 μm) was used for PLD (a pulse duration of 15 ns, a repetition rate of 25 Hz, and pulse energy of 25 mJ). The fluence in the laser spot was ~7 J/cm^2. The laser plume was directed along the normal toward the substrate surface. The deposition chamber was evacuated to a pressure of ~10^{-4} Pa. Hereinafter throughout the text, PLD at a pressure of ~10^{-4} Pa will be referred to as PLD in vacuum conditions. In some experiments, the buffer gas Ar was introduced into the chamber after evacuation. The pressure of Ar was 2 or 10 Pa. This option will be denoted as PLD in Ar. Prior to the PLD, the $MoSe_2$ target was repeatedly irradiated by the laser pulses. The substrate was protected from laser plume deposition using a shutter. Pulsed laser pretreatment was used to modify the polished surface layer of the target and to induce the formation of Mo nanoparticles in this layer. After removing the shutter, the nanoparticles were deposited on the substrate.

Surface morphology of the $MoSe_2$ target was characterized by a scanning electron microscope (SEM, Tescan Lyra 3) equipped with an energy dispersive spectroscope (EDS). The SEM and EDS analyses were made on the surfaces of the pressed target, the mechanically polished target and the laser irradiated target.

The $MoSe_x$/nc-Mo coatings were deposited on substrates made from polished silicon wafers (Si), NaCl crystals, and polished stainless steel (Cr 18%) disks. The deposition was done on substrates that were heated to 250 °C. The average thickness of coatings on the steel substrates was ~0.3 μm.

The structure of $MoSe_x$/nc-Mo films, deposited on NaCl substrates, was studied using transmission electron microscopy and micro-diffraction (TEM and MD, JEM-200EX, Jeol, Japan, operating voltage 200 kV). The films were first planted in water using a metal mesh, and were then transferred to the microscope in order to obtain a planar image. The structure and phase composition of coatings, deposited on Si substrates, were investigated by means of X-ray diffraction (XRD, CuKα radiation). The surface topography of these coatings was examined by atomic force microscopy (AFM, Solver Pro-M, NT-MDT, Russia) in the contact mode under ambient conditions.

The tribological properties of the coatings deposited on the steel substrates were evaluated using a conventional ball-on-disk tribometer (CSM Instruments, Switzerland) under a normal load of 1 N with a 3-mm diameter 100Cr6 ball as a counterpart material. Three tests were performed on each sample with the wear track diameter varied within the range of 0.6–1.0 cm. Sliding speed was 10 cm/s. Friction tests were conducted in air with relative humidity of ~ 40%. Wear tracks were analyzed using an optical microscope.

3. RESULTS AND DISCUSSION

3.1. Modification of $MoSe_2$ Target Surface Under Pulsed Laser Irradiation

Figure **1** shows SEM images and EDS spectra measured on the surface of the $MoSe_2$ target before and after the mechanical polishing followed by the pulsed laser irradiation. The pressed target was composed of $MoSe_2$ microcrystals having a lamellar shape. EDS measurements showed that the elements (Mo and Se) were fairly uniformly distributed throughout the volume of the microcrystals (Figure **1a**). Chemical composition of the synthesized microcrystals was equal to a stoichiometric value (x~2). Mechanical polishing resulted in smoothing of the target surface (Figure **1b**). After the mechanical treatment, the surface layer of the target contained a surplus Se (x~14). Particles of micrometer size with spheroidal shape were formed on the polished target surface. The chemical composition of these particles was close to stoichiometric.

Laser irradiation caused the surface layer of the $MoSe_2$ target to melt (Figure **1c**). The melted surface contained deep cavities and high protrusions, which were covered by spherical (ball-shaped) particles of micrometer and nanometer sizes. For the target irradiated by a single laser pulse, EDS analysis showed that Se concentration decreased to some extent (x~6) and the chemical composition x of the particles varies in a range 2.1 – 5.5. After the target irradiation with multiple laser pulses, the surface concentration of the particles of micrometer sizes decreased and the ball-shaped particle of submicrometer and nanometer sizes were formed extensively (Figure **1d**). The Se concentration in the melted surface layer decreased to a
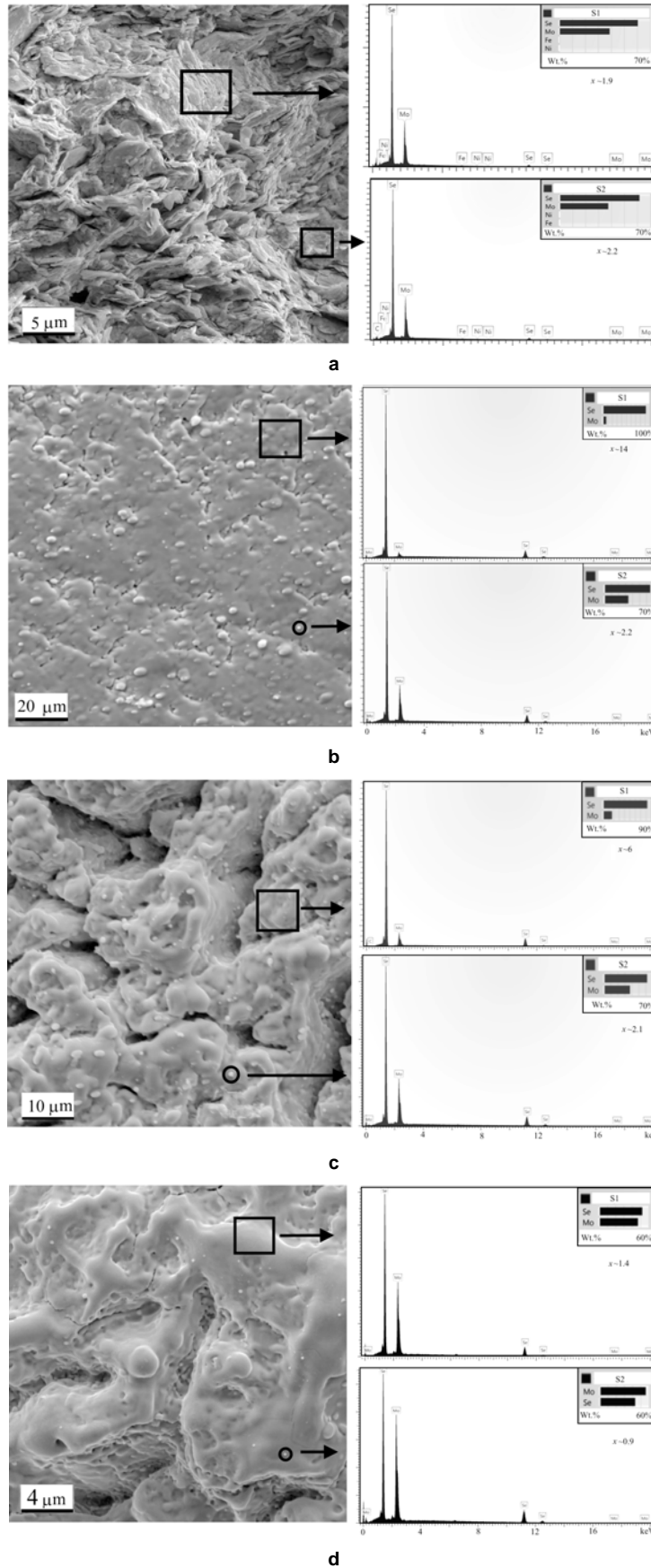
Figure 1: SEM images and EDS spectra of marked areas for (**a**) pressed MoSe$_2$ target; (**b**) polished MoSe$_2$ target; (**c**) polished MoSe$_2$ target after irradiation by single laser pulse; (**d**) polished MoSe$_2$ target after irradiation by 20 laser pulses.

substoichiometric value ($x\sim1.4$) and the ball-shaped particles were enriched with Mo ($x\sim0.9$).

Several mechanisms responsible for the formation of Mo-enriched particles can be proposed. During pulsed laser irradiation of the $MoSe_2$ target, 1.06 µm wavelength light penetrated to a depth of ≥0.1 µm [10]. At the initial stage of pulsed laser exposure, this layer was subject to intense and rapid heating [11]. The selenium could preferentially evaporate and the surface layer of the target could be enriched with Mo. Due to surface metallization, the laser absorption coefficient increased [12, 13]. The "explosion" of the thin metal film covering the target could induce the formation of Mo particles. Some of the particles remained on the surface, but some emitted from the target and deposited on the substrate. Relatively large Mo particles could form on the target surface because of the coalescence of Mo nanoparticles. Preferential Mo condensation from a laser-induced vapor could also cause the Mo nanoparticles formation on the target surface.

Yavsin *et al.* [14] proposed another mechanism of nanoparticle formation during PLD. The effective melting and evaporation of the target material by laser irradiation could be followed by optical breakdown of the vapor. The melted layer on the target surface is in the pressure field of the laser-induced plume, which results in the development of a capillary instability in this layer and the ejection of submicrometer droplets from the target surface. Upon entering the laser-induced plasma, these droplets are charged to a floating potential whose value is proportional to the electronic temperature of the plasma. At a sufficiently high plasma temperature, the charge of the droplets becomes so large that the Coulomb repulsion force exceeds the surface tension force, with the droplet losing its spherical shape and starting to divide into a number of smaller droplets. The division process has a cascade nature and abruptly stops at droplet sizes on the order of several nanometers, when the droplets lose their charge because of increasing field-emission current from their surface. The resulting "nanodroplets" are deposited onto a substrate.

It is also possible that the Mo nanoparticles are growing in the bulk of the melted layer. The ultra fast laser heating caused the formation of a superheated/metastable liquid phase in the relatively thick surface layer of the target. During the cooling of this alloy, Mo precipitation could occur, since the equilibrium phase diagram eliminates the possibility of Se mixing with Mo in the melt [15]. The resulting precipitates were then "frozen" in the surface layer. Repeated laser irradiation caused the surface layer to evaporate, such that the Mo precipitates could be captured by the steam formed by laser ablation, and transferred to the substrate.

A hydrodynamic mechanism of nanoparticle formation includes the creation of a molten surface layer by laser irradiation that was accompanied by an acceleration of the melt surface due to volume change. The Rayleigh-Taylor

instability could cause the formation of waves on the melt surface [12]. The wave parameters depended on the magnitude of the acceleration, the thickness of the liquid phase layer, and the surface tension of the melt layer. If the metastable $MoSe_x$ melt is severely overheated, the surface tension can be reduced significantly, and as a result, a periodic structure could be formed, having a short wavelength. In this case, $MoSe_x$ nanoparticles can break off from the molten $MoSe_x$ target surface layer. The Se content in these nanoparticles can depend on many factors, but most likely it will be significantly less than stoichiometric. This is due to the effective Se desorption at high temperatures under vacuum conditions.

It should be noted that the deposition of the $MoSe_x$/nc-Mo coatings was performed at a relatively low pressure of the buffer gas. Therefore, a mechanism of nanoparticles formation due to the condensation of the laser plume during its movement from the target to the substrate [16] was not considered in this discussion.

3.2. Structure and Chemical Composition of the $MoSe_x$/nc-Mo Coatings

Comprehensive study of the coatings deposited on the Si and NaCl substrates confirmed the fact that nanoparticles, which were formed during pulsed laser irradiation of the $MoSe_2$ target, have caused the modification of the structure and phase composition of the obtained coatings. The results of TEM and MD studies of the $MoSe_x$/nc-Mo film deposited in vacuum conditions are shown in Figure **2**. For the films deposited in Ar and in vacuum, the main results of TEM/MD studies were similar. TEM contrast analysis of the $MoSe_x$/nc-Mo films showed that they were composed of two phases: the
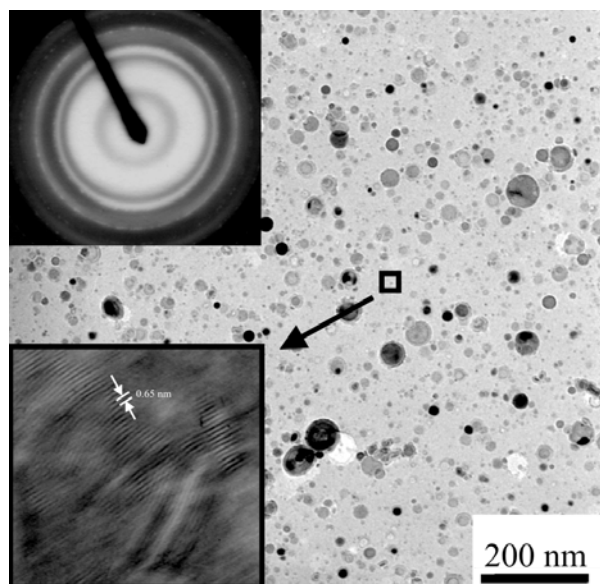
Figure 2: TEM micrograph and MD pattern (inset) of $MoSe_x$/nc-Mo film prepared using PLD in vacuum from the $MoSe_2$ target. High-resolution TEM micrograph of the marked area shows the layered structure of $MoSe_x$ matrix.

Grigoriev et al.

$MoSe_x$ matrix and spherical nanoparticles. The size of the nanoparticles varied from a few nanometers to ~50 nm. MD studies showed that the nanoparticles were composed of Mo crystals with a bcc lattice. The $MoSe_x$ matrix crystallized into a layered structure. The distance between the atomic layers was ~0.65 nm. Highly disordered atomic packing in the $MoSe_x$ nanocrystals caused a diffuse character of reflections detected in the MD pattern.

The results of XRD studies of the $MoSe_x$/nc-Mo coatings are shown in Figure **3**. For comparison, the XRD spectrum of the $MoSe_2$ target is presented. An X-ray diffraction analysis indicated dominating of a relatively narrow line in the XRD spectra of all the coatings, which corresponded to reflection from basal planes (002) of the hexagonal $2H$-$MoSe_2$ phase. Such a kind of XRD spectra is characteristic for highly oriented TMD coatings with turbostratic structure, where basal planes are oriented parallel to the surface ((001) texture). Atomic planes (002) can be oriented at an arbitrary angle around c-axis. Reflections from bcc Mo phase were found in XRD spectra also. With the increase of Ar pressure in the deposition chamber the peak intensity associated with Mo phase increased. This fact confirmed the assumption that the buffer gas can affect the concentration of Mo nanoparticles in the coatings due to the atomic flux scattering in collisions with molecules of the buffer gas [17].
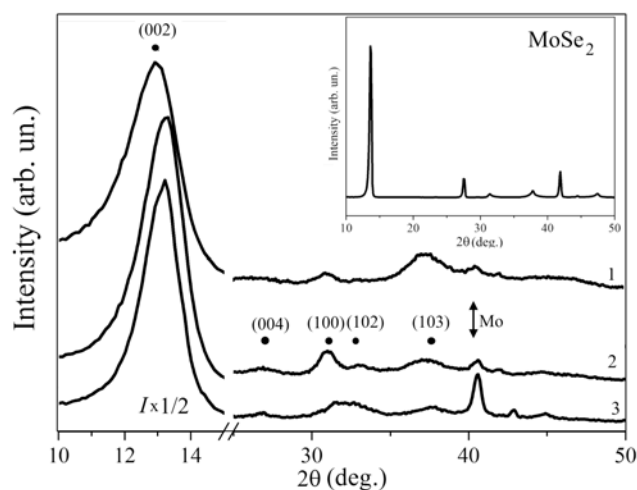
Figure 3: XRD patterns of $MoSe_x$/nc-Mo coatings prepared by PLD in vacuum (1), in Ar at 2Pa (2), and in Ar at 10 Pa (3). The lines corresponding to bcc Mo (110) and hexagonal $2H$-$MoSe_2$ phase are denoted. The insert shows the XRD pattern of $MoSe_2$ target.

The increase of a buffer gas pressure caused the modification of the structure of matrices in the composite $MoSe_x$/nc-Mo coatings. For comparison with the vacuum-deposited coatings, the Ar gas at 2 Pa caused the modification of XRD spectra, resulting in the sharpening of (002) reflection and its shift to higher diffraction angles. For Ar pressure of 10 Pa, this reflection was broadened noticeably. This indicated that the (002) spacing decreased from 0.687 nm to 0,671 nm, i.e., the distance between the basic atomic planes approached to the tabulated value of

0.646 nm. A relatively broad asymmetric peak with a long tail representing a turbostratic stacking of $10l$ (l = 0, 1, 2, 3) planes demonstrated the narrowing/intensification of the (100) line in Ar at 2 Pa, and the broadening/shifting of this and other lines in Ar at 10 Pa.

This observation allows suggesting an improvement of structural ordering in the $MoSe_x$/nc-Mo coatings prepared in Ar at 2Pa in comparison with the vacuum-deposited coatings, as well as with the coatings deposited in Ar at 10 Pa. Weise *et al.* [18] calculated the scattering curves of simulated model structure for nanocrystalline TMD materials. The calculation showed that the intensity and the shape of the $(00l)$ reflections are determined by the number and the extent of stacking of a-b basal lattice planes in the c direction. The $(hk0)$ reflections are correlated with the range of ordering of the atoms in the a-b planes. For the line (100), the decrease of the size of the model nanocrystals causes the increase of the line width and the decrease of its intensity. The line is shifted to higher angles of reflection.

The modification of the matrix structure in the buffer gas happens due to the next PLD feature: the growing coating is bombarded by high-energy atomic particles (neutral atoms and ions). The energy of these particles reaches several hundreds of eV. The buffer gas with the pressure greater or equal to 2 Pa considerably influences the dose of irradiation by high-energy atomic particles, as well as the energy and angle distributions of the atomic particles during deposition [19, 20]. The bombardment can initiate a number of competitive processes on the surface and in the bulk of the $MoSe_x$/nc-Mo coating. Defect zones are formed on the surface of the coating with the basal orientation serving as nucleation centers, which are favorable for (001) texture formation. On the other hand, $MoSe_x$ nanocrystals with basal orientation are more sensitive to bombardment-induced amorphisation, than the nanocrystals with basal planes perpendicular to the surface (parallel to the direction of high-energy particles). The used Ar gas with the pressure of about 2 Pa appears to optimize the bombardment dose and to change the mechanism of coating matrix growth. It has to be noticed that the Se concentration in $MoSe_x$-based coatings increases at PLD in Ar and it equals to stoichiometric value at the Ar pressure of 2 Pa [19]. The increase of the pressure up to 10 Pa resulted in an essential decrease of the energy of deposited atoms, which fall on the coating surface under large angles (relative to perpendicular). These facts can cause a decrease of the coating density [21].

The deposition of nanoparticles had an obvious influence on the formation of roughness of coatings surfaces. Figure **4a** shows the AFM image of the $MoSe_x$/nc-Mo coatings prepared in the vacuum conditions. Relatively small nanoparticle (sizes ~5 – 10 nm) cover the surface densely but the bigger particles (~20 – 40 nm) have random distribution on the surface. When the deposition of the coatings was carried out in Ar buffer gas, the coalescence of nanoparticles and the deposition of atomic flux on the attached particles elicited the

formation of hill-shaped protrusions, which heights reached 100 nm, and their lateral sizes were ~ 200 nm (Figure **4b**). For the vacuum-deposited coatings, the root mean square roughness was ~8.9 nm. The increase of the nanoparticle content during the deposition in Ar buffer gas caused the increase of the surface roughness up to 9.9 nm and 11.2 nm for the coatings deposited at 2 and 10 Pa, respectively.

a

b
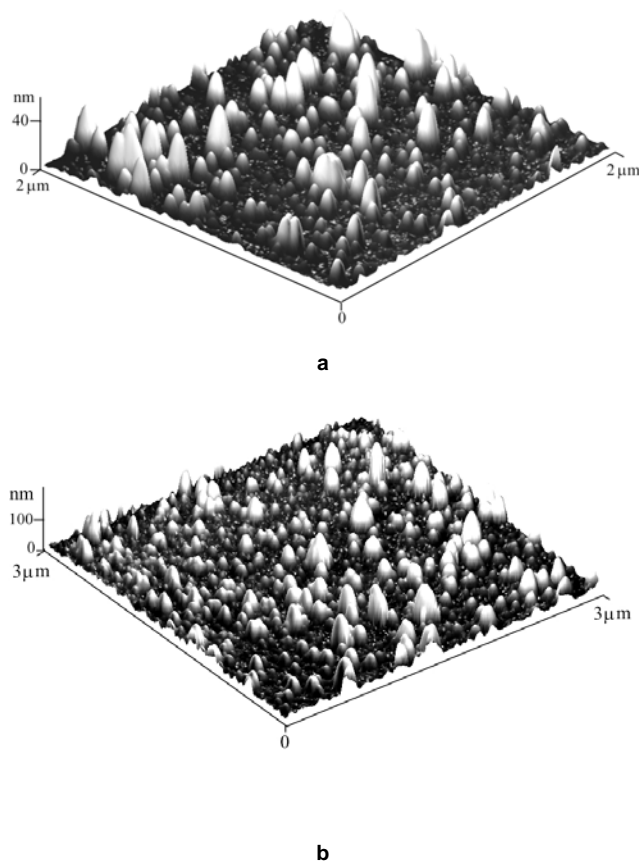
Figure 4: AFM image of the surface of MoSe$_x$/nc-Mo coatings prepared using PLD (**a**) in vacuum and (**b**) in Ar at 10 Pa.

3.3. Tribological properties of the MoSe$_x$/nc-Mo coatings

For the prepared MoSe$_x$/nc-Mo coatings, the results of tribological tests are shown in Figures **5** and **6**. The coefficient of friction was weakly dependent on the concentration of the nanoparticles. The average value of the friction coefficient decreased down to 0.04 after running-in (Figure **5**). However, the coatings wear decreased when the Ar gas was added to the pressure of 2 Pa, and then the coatings wear increased with the pressure growth from 2 Pa to 10 Pa.

The MoSe$_x$/nc-Mo coating deposited in vacuum were removed from the steel substrate after 6×10^3 cycles of sliding and the wear of the steel substrate started to develop (Figure **6a**). The wear rate of this coating was about 7×10^{-6} mm^{3}N^{-1}m^{-1}. For the MoSe$_x$/nc-Mo coating deposited in Ar at 2 Pa, the coating material is retained in the wear track after even 1.5×10^4 cycles. The coefficient of friction varied in

a

b

c
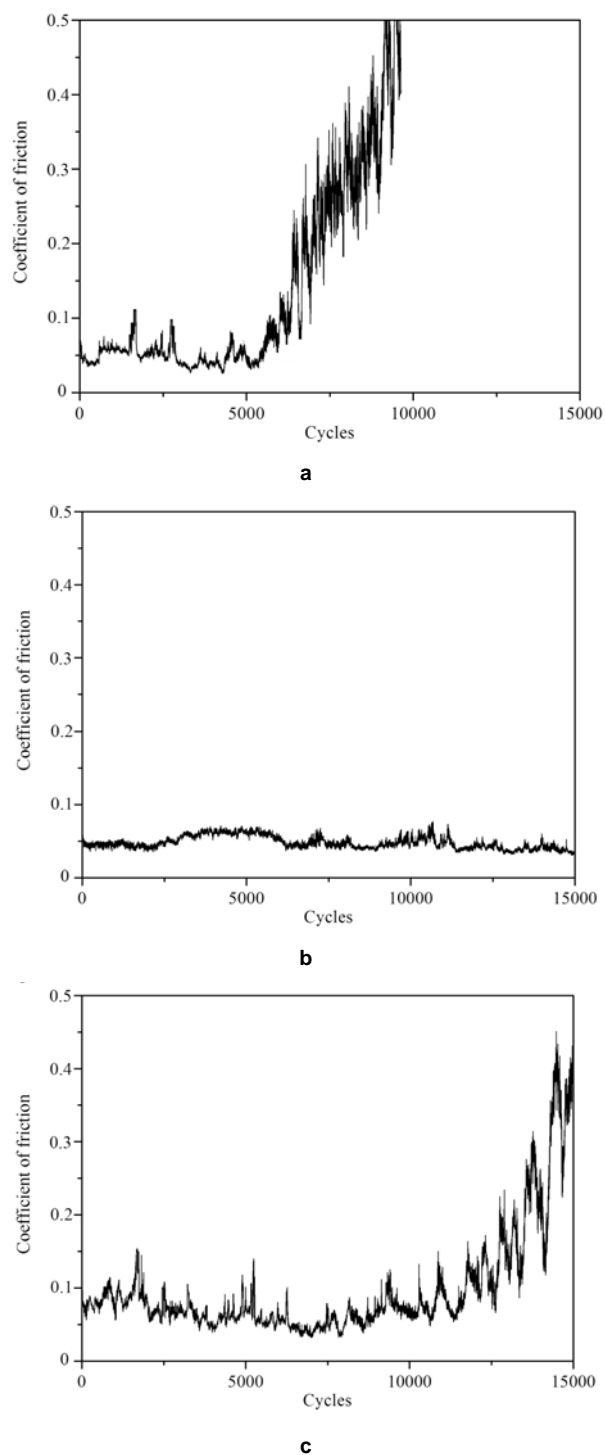
Figure 5: Coefficient of friction *vs*. cycles of sliding for MoSe$_x$/nc-Mo coatings prepared using PLD in (a) vacuum; (b) Ar at 2 Pa; and (c) Ar at 10 Pa.

the range 0.04 – 0.06 during the whole sliding process and the wear of the steel substrate was not detected (Figure **6b**). The wear rate of this coating was ~6×10^{-7} mm^{3}N^{-1}m^{-1}. The increase of the Ar pressure to 10 Pa resulted in a deterioration of the tribological properties. The coefficient of friction had frequent fluctuations and the wear of the steel substrate began after 1.2×10^4 cycles. Nevertheless, the

coating material is retained on lateral edges of the wear track after 1.2×10^4 cycles (Figure **6c**).
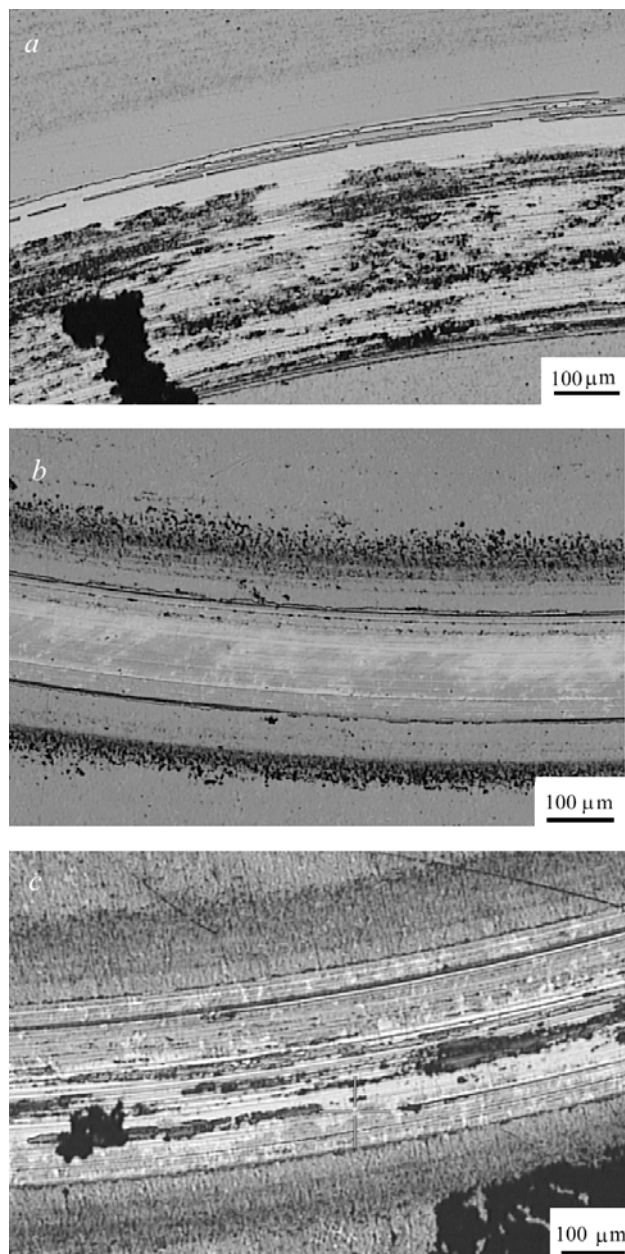
Figure 6: Optical micrographs of the wear tracks formed on steel with MoSe$_x$/nc-Mo coatings prepared using PLD in (**a**) vacuum, (**b**) Ar at 2 Pa, and (**c**) Ar at 10 Pa. The tracks were analyzed after 6×10^3, 1.5×10^4, and 1.2×10^4 cycles, respectively.

Thus, the increase of the concentration of Mo nanoparticles following the Ar pressure increase could result in the decrease of the coating wear. The analysis of the wear tracks allows assuming that the wear mechanism of the MoSe$_x$/nc-Mo coatings changed from abrasion (vacuum deposition) to adhesion (deposition in Ar) wear due to an intensive formation of tribofilm on the surface of wear tracks. The features of the wear dynamics of the prepared in Ar coatings, which are very weak wear of the substrate under thinning of the coating and conservation of the low value of the

coefficient of friction could be due to the nanostructural characteristics of the coating. During gradual wear of this coating, the hard ball-shaped Mo particles probably moved to the deeply lying layers and located at the boundary with the substrate. The thickness of such a layer is probably comparable with the size of the Mo nanoparticles and could be several tens of nanometers. The conservation of the solid lubricant MoSe$_x$ phase in the environment of "nanoballs" provided their efficient displacement with the rotation in the contact region. As a result, on the one hand, the direct contact of the steel ball with the substrate was excluded; on the other hand, the tribological modification of the contact surfaces occurred. The structural and compositional properties of the solid lubricant MoSe$_x$ matrix could play an essential role in the wear mechanism. The realized conditions of the deposition of MoSe$_x$/nc-Mo coating in Ar at 2 Pa facilitated the best performance of the matrix.

Domínguez-Meister *et al.* [22] have obtained the low friction coatings containing a composition of TMD nanocrystals with metal-based amorphous phase. This nanocomposition of the coatings allowed implementing low friction (0.07) and low wearing rate (3×10^{-7} mm^{3}N^{-1} m^{-1}) even in ambient air. The metal atoms played a sacrificial role preventing the lubricant phase oxidation. The comparison of tribological properties of the nanocomposite TMD-based coatings exhibiting different architecture/design could help to understand the role of ball-shaped nanoparticle in the wear mechanisms better. However, the real comparative tribological tests are needed to make valid conclusions in the field.

4. CONCLUSION

The specific non-equilibrium conditions, that are realized on the surface of the MoSe$_2$ target under the irradiation by laser pulses of ~10 ns duration, cause the formation of spherical nanoparticles of Mo, which are transported by laser plume and then fall on the substrate. Co-deposition of the laser-induced vapor and nanoparticles resulted in the formation of nanocomposite coatings with the new design. The MoSe$_x$/nc-Mo coatings contained ball-shaped crystalline Mo nanoparticles distributed in the solid lubricant MoSe$_x$ matrix. The size of Mo particles varies in the range of about 5 - 50 nm.

The increase of buffer gas pressure resulted in the increase of Mo nanoparticles content in the MoSe$_x$/nc-Mo coatings. Unfortunately, the buffer gas influenced the structural and compositional properties of the MoSe$_x$ matrix also. Therefore, in order to obtain a coating with superior properties, an optimal condition of PLD (the laser fluence and number of laser pulses for target ablation, the pressure and composition of buffer gas, and etc.) should be determined. The MoSe$_x$/nc-Mo coatings prepared in Ar at 2 Pa possessed the best performance including the most stable and lowest friction coefficient during the all test.

The Mo nanoparticles could change the wear mechanism due to some processes in the area of tribo contact: the rotational

motion of the hard ball-shaped particles, the conservation of solid lubricant $MoSe_x$ material in the tribofilms, and the hardening of the nanocomposite coatings. The increase of the crystalline order of the $MoSe_x$ matrix having the perfect chemical composition ($x{\sim}2$) as well as a multifactor effect of Mo nanoparticles would explain the enhanced tribological response of the $MoSe_x$/nc-Mo coatings prepared in Ar at 2 Pa.

ACKNOWLEDGEMENTS

REFERENCES

[1] Polcar T, Cavaleiro A. Review on self-lubricant transition metal dichalcogenide nanocomposite coatings alloyed with carbon. Surf Coat Technol 2011; 206: 686-95.
http://dx.doi.org/10.1016/j.surfcoat.2011.03.004

[2] Fominski VY, Grigoriev SN, Gnedovets AG, Romanov RI. Pulsed laser deposition of composite Mo–Se–Ni–C coatings using standard and shadow mask configuration. Surf Coat Technol 2012; 206: 5046-54.
http://dx.doi.org/10.1016/j.surfcoat.2012.06.004

[3] Polcar T, Cavaleiro A. Self-adaptive low friction coatings based on transition metal dichalcogenides. Thin Solid Films 2011; 519: 4037-44.
http://dx.doi.org/10.1016/j.tsf.2011.01.180

[4] Bondarev AV, Kiryukhantsev-Korneev PV, Sheveyko AN, Shtansky DV. Structure, tribological and electrochemical properties of low friction TiAlSiCN/MoSeC coatings. Appl Surf Sci 2015; 327: 253-61.
http://dx.doi.org/10.1016/j.apsusc.2014.11.150

[5] Xu S, Gaoa X, Hu M, et al. Nanostructured WS$_2$–Ni composite films for improved oxidation, resistance and tribological performance. Appl Surf Sci 2014; 288: 15-25.
http://dx.doi.org/10.1016/j.apsusc.2013.09.024

[6] Fominski VY, Grigoriev SN, Romanov RI, Volosova MA, Demin MV. Chemical composition, structure and light reflectance of W-Se and W-Se-C films prepared by pulsed laser deposition in rare and reactive buffer gases. Vacuum 2015; 119: 19-29.
http://dx.doi.org/10.1016/j.vacuum.2015.04.031

[7] Sen R, Govindaraj A, Suenaga K, et al. Encapsulated and hollow closed-cage structures of WS$_2$and MoS$_2$ prepared by laser ablation at 450–1050ºC. Chem Phys Lett 2001; 340: 242-8.
http://dx.doi.org/10.1016/S0009-2614(01)00419-5

[8] Fominski VY, Grigoriev SN, Gnedovets AG, Romanov RI. On the mechanism of encapsulated particle formation during pulsed laser deposition of WSe$_x$ thin-film coatings. Techn Phys Let 2013; 39: 312-5.
http://dx.doi.org/10.1134/S1063785013030206

[9] Hu JJ, Zabinski JS, Bultman JE, Sanders JH, Voevodin AA. Encapsulated nanoparticles produced by pulsed laser ablation of MoS$_2$-Te composite target. Cryst Growth Des 2008; 8: 2603-5.
http://dx.doi.org/10.1021/cg7008144

[10] Feng L, Li N, Liu Z. Effect of radio frequency power on composition, structure and optical properties of MoSe$_x$ thin films. Physica B 2014; 444: 21-6.
http://dx.doi.org/10.1016/j.physb.2014.03.026

[11] Morozov AA, Evtushenko AB, Bulgakov AV. An analytical continuum-based model of time-of-flight distributions for pulsed laser ablation. Appl Phys A 2013; 110: 691-6.
http://dx.doi.org/10.1007/s00339-012-7187-9

[12] Fominski VY, Romanov RI, Smurov I, Smirnov AL. Surface alloying of metals by nanosecond laser pulse under transparent overlays. J Appl Phys 2003; 93: 5989-99.
http://dx.doi.org/10.1063/1.1568149

[13] Morozov AA. Analytical formula for interpretation of time-of-flight distributions for neutral particles under pulsed laser evaporation in vacuum Analytical formula for interpretation of time-of-flight distributions for neutral particles under pulsed laser evaporation in vacuum. J Phys D: Appl Phys 2015; 48: 195501.
http://dx.doi.org/10.1088/0022-3727/48/19/195501

[14] Yavsin DA, Kozhevin VM, Gurevich SA, et al. Nanostructured Ge$_2$Sb$_2$Te$_5$ chalcogenide films produced by laser electrodeposition. Semiconductors 2014; 48: 1567-70.
http://dx.doi.org/10.1134/S1063782614120239

[15] http://www.himikatus.ru/art/phase-diagr1/Mo-Se.php

[16] Safronov AP, Beketov IV, Komogortsev SV, et al. Spherical magnetic nanoparticles fabricated by laser target evaporation. AIP Advances 2013; 3: 052135.
http://dx.doi.org/10.1063/1.4808368

[17] Grigoriev SN, Fominski VY, Romanov RI, Gnedovets AG, Volosova MA. Shadow masked pulsed laser deposition of WSe$_x$ films: Experiment and modeling. Appl Surf Sci 2013; 282: 607-14.
http://dx.doi.org/10.1016/j.apsusc.2013.06.020

[18] Weise G, Mattern N, Hermann H, et al. Preparation, structure and properties of MoS$_x$ films. Thin Solid Films 1997; 298: 98-106.
http://dx.doi.org/10.1016/S0040-6090(96)09165-1

[19] Fominski VY, Romanov RI, Gnedovets AG, Nevolin VN. Formation of the chemical composition of transition metal dichalcogenide thin films at pulsed laser deposition. Techn Phys 2010; 55: 1509-16.
http://dx.doi.org/10.1134/S106378421010018X

[20] RashidianVaziri MR, Hajiesmaeilbaigi F, Maleki MH. Microscopic description of the thermalization process during pulsed laser deposition of aluminum in the presence of argon background gas. J Phys D: Appl Phys 2010; 43: 425205.
http://dx.doi.org/10.1088/0022-3727/43/42/425205

[21] Nevolin VN, Fominski VY, Gnedovets AG, Romanov RI. Pulsed laser deposition of thin-film coatings using an antidroplet shield. Techn Phys 2009; 54: 1681-8.
http://dx.doi.org/10.1134/S1063784209110218

[22] Domínguez-Meister S, Conte M, Igartua A, Rojas TC, Sánchez-López JC. Self-lubricity of WSe$_x$ nanocomposite coatings. ACS Appl Mater Interfaces 2015; 7: 7979-86.
http://dx.doi.org/10.1021/am508939s